IEEE Photonics Journal
An IEEE Photonics Society Publication

Open Access

Efficient Color Filters Based on Fano-Like Guided-Mode Resonances in Photonic Crystal Slabs

Volume 10, Number 1, February 2018

Van An Nguyen
Quang Minh Ngo, *Member, IEEE*
Khai Quang Le, *Member, IEEE*

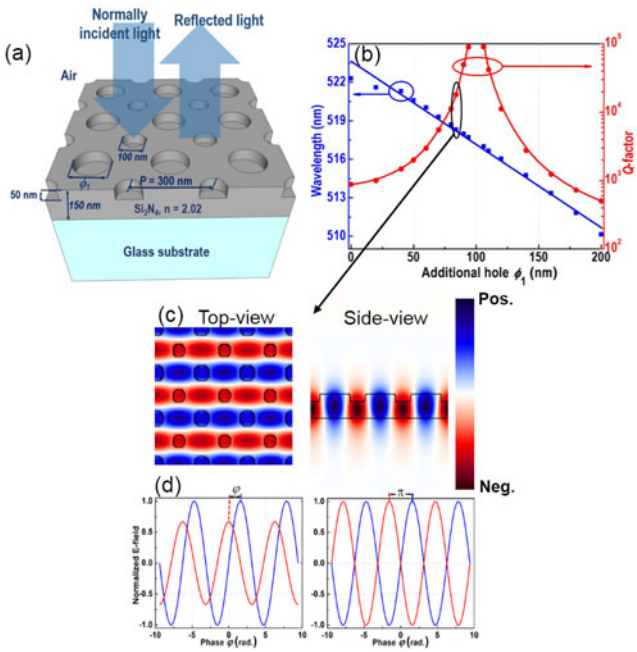

DOI: 10.1109/JPHOT.2018.2796566
1943-0655 © 2018 IEEE

IEEE photonics SOCIETY

IEEE

Efficient Color Filters Based on Fano-Like Guided-Mode Resonances in Photonic Crystal Slabs

Van An Nguyen,[1,2] Quang Minh Ngo [1,2] *Member, IEEE*, and Khai Quang Le [3,4] *Member, IEEE*

[1]Institute of Materials Science, Vietnam Academy of Science and Technology, 18 Hoang Quoc Viet, Cau Giay, Hanoi, Vietnam
[2]Graduate University of Science and Tecnology, 18 Hoang Quoc Viet, Cau Giay, Hanoi, Vietnam
[3]Division of Computational Physics, Institute for Computational Science, Ton Duc Thang University, Ho Chi Minh City, Vietnam
[4]Faculty of Electrical and Electronics Engineering, Ton Duc Thang University, Ho Chi Minh City, Vietnam

DOI:10.1109/JPHOT.2018.2796566

Manuscript received January 3, 2018; revised January 17, 2018; accepted January 18, 2018. Date of publication January 23, 2018; date of current version April 5, 2018. This research is funded by Vietnam National Foundation for Science and Technology Development (NAFOSTED) under grant number "103.03-2017.02." Corresponding author: Q. M. Ngo (e-mail: minhnq@ims.vast.ac.vn).

Abstract: We numerically report designs of color filters comprising of 2-D photonic crystal (2D-PhC) slabs of square lattice of air holes. The filter principle is based on excited Fano-like guided-mode resonances (GMRs) in the visible regime with high-quality factor (*Q*-factor) and low reflection sidebands. The 2D-PhC slab architecture influence on its spectroscopic property is comprehensively investigated. We introduce an alternative PhC lattice, which is formed by introducing an additional hole in each unit cell to enhance the light confinement in the waveguide slab, as such the induced Fano-like GMRs' *Q*-factor is significantly increased about two orders of magnitude compared to the traditional PhC without additional holes. At Fano-like GMRs, two in-plane waves oscillate toward the opposite directions with a phase difference of π. The radiated fields of these waves strongly cancel each other in the far field, and the coupling between the waveguiding slab and the incident light is dramatically reduced resulting in the high *Q*-factor of the Fano-like GMR in the introduced PhC slab. As a result, the 2D-PhC slab excited Fano-like GMRs in this work may find fascinating applications in optical filters, optical imaging, optical switching, and so on.

Index Terms: Subwavelength structures, integrated optic devices, color filters.

1. Introduction

An optical color filter is a key component for many optical devices such as optical image sensors in charge coupled devices, crystal shutters in line sensors and display devices including televisions, computers, mobile phones, digital cameras, e-readers [1]–[3]. Numerous materials have been studied in the past to realize color filters such as dyes, pigments, and metals. However, color filters based on dyes and pigments are limited because of their low efficiency, thermal loss, absorption, and selective color imperfectly where the colors are produced by the exchange of energies between photons and electrons [2], [4]. Recently, engineered color filters employing photonic/plasmonic nanostructures have been studied extensively. In general, these color filters are mainly based on several elementary optical processes including reflection, refraction, interference,

diffraction, scattering and so on within the microscale structures. For the display components, the engineered color filters are brighter under light illumination, more free from photobleaching, and flexible tunable than dye or pigmentary colors [3], [5]–[11]. Engineered color filters based on plasmon effects in metallic and metamaterial nanostructures have been undertaken attractively owing to their promising features including planar geometry with thin thickness, and full color display [7], [9]. Unfortunately, metal suffers from inherent losses in the visible spectrum. Its optical spectroscopies induced by plasmonic effects are typically broadband with low *Q*-factor and less intensive. In addition, plasmonic colors are angularly sensitive. The Q-factor is defined as a ratio between the resonant wavelength over the resonant linewidth at half-maximum (FWHM). To circumvent this problem, metal-free engineered color filters using dielectric GMR refractive filters have been introduced in the past decade [5]–[7], [12]–[14]. Various dielectric engineered structures excited GMRs have been reported including slab waveguide gratings (WGs) and normal PhC slabs. They provided high color efficiency with highly tunable bandwidth. The GMR spectroscopy usually has Lorentzian shape, which exhibits strong reflection peak (nearly unity), high spectral contrast (low reflection sidebands), flexible in material choice, suitable for large scale fabrication, weak angular dependence, and dynamic tuning of the reflectance spectrum.

Alternative GMRs with Fano shape have been investigated in slab WGs and normal PhC slabs [5], [15], [16]. In contrast to Lorentzian GMRs, Fano GMR is excited by the coupling between guided-mode in the slab (discrete state) and external radiation (continuum background) constituting in this way an efficient mechanism to transfer the guided-mode within the slab to external media. Recently, GMRs in slab WGs and PhC slabs have been designed and fabricated to get the different resonant Lorentzian and Fano lineshapes with low reflection sidebands from the visible to near-infrared spectral regions, which applied for polarization-controlled tunable colors, near infrared filters, and optical switching/bistability [5], [17]–[21]. While slab WGs are sensitive to the incoming light polarization, the normal PhC slabs weakly depend on the polarization stabilization of the light source as shown in [22]–[25]. In these PhC slabs, the resonant wavelength and the *Q*-factor of the excited GMRs are insensitive to the normally incident light polarization. Significant advantages of Fano-like GMRs are related to their high *Q*-factor and ability to enhance it. First, the Fano-like optical filter's *Q*-factor can be 10^4 in single-layer PhCs and can be increased up to over 10^7 by using stacked double-layer PhC configurations [17], [18]. Second, an alternative PhC slab structure was generated by introducing a rectangular slot in each unit cell of the Suzuki-phase lattice to enhance the electromagnetic field confinement of the GMRs. The calculated *Q*-factor in an ideal structure is over 4×10^5. This structure shows a flatter band at the Γ-point compared with the normal PhC slabs [23], [24], [26]. However, this structure is highly dependent on the polarization of incident light. In this work, we introduce an alternative PhC structure which is formed by introducing additional hole in each unit cell to create and maintain the interaction of two in-plane waves oscillated towards the opposite direction of phase difference of π. It is seen that the radiated fields of two in-plane waves strongly cancel each other out in the far field, and the coupling between the waveguiding slab and the incident light is largely minimized thanks to interference between reflected back and forth at the GMR, resulting in a high *Q*-factor of Fano-like GMR. Large *Q*-factor on an order of $\sim 10^5$ or higher can be achieved by tuning the structural parameters and size of the additional hole. It is two orders of magnitude larger than that of the structure without introducing hole in the center. In addition, the proposed PhC lattice is a symmetry structure at normally incident light, so that it is independent on the incident light polarization. The resulting Fano-like GMRs may find applications in optical filters, optical imaging, and optical switching, and our investigation on the dependence of the structural parameters, incident polarization and angles on resonant shapes and *Q*-factors will provide a general guideline for free-space optical devices. All numerical simulations were carried out by the finite-difference time-domain (FDTD) method with subpixel smoothing for increased accuracy [27], [28].

2. Color Filters Based on Fano-Like GMRs in Normal PhC Slabs

A slab structure whose high-index layer is silicon nitride material (Si_3N_4, $n = 2.02$) with thickness t deposited on the glass substrate is depicted in Fig. 1(a). A normal PhC slab is formed by a square

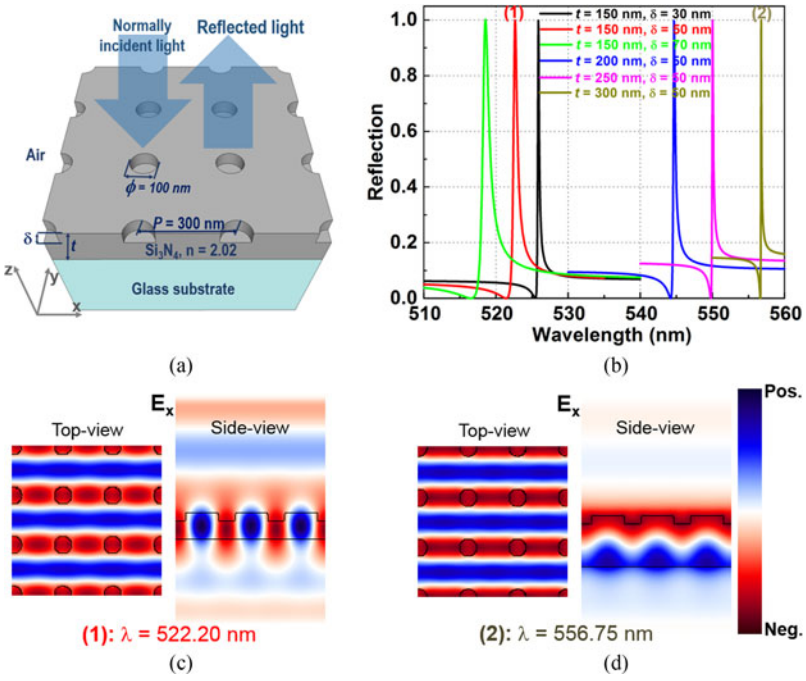

Fig. 1. (a) Sketch of a normal PhC slab structure of square lattice of air holes on high-index layer under normally incident light. (b) Reflection spectra for various slab thicknesses (t) and hole depths (δ). (c) and (d) show the electric field distributions along x direction of top- and side-views at the resonances for slab thicknesses of 150 nm and 300 nm, respectively. The parameters of structure of $P = 300$ nm and $\phi = 100$ nm are chosen for the simulated results.

lattice (lattice constant $P = 300$ nm) of air holes (diameter $\phi = 100$ nm) with a depth of δ perforated in a Si_3N_4 layer.

Fig. 1(b) shows the calculated linear reflection spectra for various depths δ. Since normal PhC slabs are insensitive to the incident light polarization [22], [29], the TE-like mode is applied as the incident plane wave. In the calculation, the perfectly matched absorbing boundary conditions are used in the top and the bottom boundaries [27]. As seen in Fig. 1(b), the reflection filters with low asymmetric sidebands and their Fano-like spectra are achieved. The figure also shows reflection spectra for various thicknesses (t) of the Si_3N_4 slab and depths (δ) of the perforated holes. For Si_3N_4 thickness $t = 150$ nm, when the hole depth δ is increased, the reflection spectrum is blue-shifted, which is caused by the reduction of the effective refractive index of the slab [30], [31] and the slab guided-mode gets strong leaky and hence, the linewidth becomes broader resulting in a decrement of Q-factor. As the depth δ is 50 nm, the Fano-like resonance is generally narrower and red-shifted for thicker Si_3N_4 slabs as shown in the same figure. This is attributed to the added optical path in the thicker slab waveguide leads to longer resonance lifetime and increment of the effective index of the slab. The characteristics of the Fano-like GMRs in normal PhC slabs for various hole depths and slab thicknesses are summarized in Table 1.

Apart from the characteristics of the Fano-like GMR in normal PhC slabs, its performance is amongst key factors to determine the color filter in which the peak wavelength, Q-, and q-factors of the optical response are needed to compute. In order to calculate these factors of the reflection spectrum, we fit the spectrum to the Fano-lineshape as follows [16]:

$$R(\varepsilon) = F\frac{(\varepsilon + q)^2}{1 + \varepsilon^2} \tag{1}$$

where $\varepsilon = 2\frac{\omega - \omega_0}{\Gamma}$, q is an asymmetric factor, ω_0 is a resonant frequency, F is a constant factor which describes the degree of asymmetry, and Γ is a resonant linewidth at half-maximum. The Q-factor

TABLE 1
Linear Characteristics of the Normal PhC Slab Filters for Several Slab Thicknesses (t) and Hole Depths (δ)

Si_3N_4 thickness (t), hole depth (δ) – nm	150 (30)	150 (50)	150 (70)	200 (50)	250 (50)	300 (50)
Peak wavelength (nm)	525.9	522.2	518.4	544.7	550.0	556.8
Quality factor Q	2459.6	879.8	525.2	1943.6	3525.0	4587.0
FWHM (nm)	0.21	0.59	0.99	0.28	0.16	0.12
Asymmetric factor q	−3.80	−3.86	−3.95	−3.02	−2.59	−2.38

is defined by the resonant frequency over the resonant linewidth at half-maximum. The Eq. (1) has been widely used to express the spectral response of Fano lineshape. It suggests that there are exactly one minimum and one maximum in the Fano lineshape. The F-factor is chosen for maximum amplitude of lineshape to unity. The lineshape is strongly determined by q-factor. Table 1 shows the calculated results of the optical characteristics of the reflection spectra for various slab thicknesses and depths. For a variation of q-factor, the degree and asymmetry of lineshape change and the actual resonant frequency locate in between the peak (maximum response) and the dip (minimum response) of the asymmetric lineshape. In addition, when q-factor changes sign, the reversible of Fano lineshape is reversed. As a consequence, both changing of amplitude and sign of q-factor hold significant implications for the promising photonic device applications such as sensitive optical filters, lasers, biosensors, and also switching/bistability [16], [20], [21].

The electric field profiles for three unit cells along the x direction at side view (x axis) and top view (z axis) exhibit the optical characteristics as shown in Fig. 1(c) and (d). The electric field distributions at the top view for the thin and thick and slab waveguide have the same forms, but their side views are different. For the thin slab waveguide ($t = 150$ nm), the electric field profile indicates that the reflection peak arises from a first order coupling to the TE_0-like mode. For the thick slab waveguide ($t = 300$ nm), the electric field profile indicates that the reflection peak arises from a first order coupling to the TE_1-like mode. The added optical path in the thicker slab waveguide makes longer resonance lifetime, or Q-factor increases [32]. The dependence of optical characteristics of color filters on the other PhC slab structures whose influenced hole sizes are not shown exhibit the same tendency.

The oblique incident angle θ_i is defined by the angle between wavevector k and the z axis. To understand the angular dependence on the optical properties, we next calculate the reflection of the structure versus to the incident angle. The slab thickness t and depth δ of 300 nm and 50 nm are chosen for the simulation, respectively. Fig. 2(a) shows the dependences of the incident angle θ_i on the reflection spectra for TE-like mode of electric field along x direction. The red hot spot around 522 nm in the figure represents a depthless in reflectivity and hence indicates the presence of a strong optical mode for the incident angle smaller than 30°. The width and blueness of the shaded area indicate the width and strength of the optical mode. Fig. 2(b) shows the example of reflectance peaks caused by Fano-like resonance for incident angles with $\theta_i = 10°$, 20°, 30°, 40°, and 50°. As Fig. 2 shown, the change of incidence angle makes only change the amplitude of reflection. It doesn't change the resonant wavelength near 522 nm. In addition, the sidebands slightly change when the incident angle changes. The numerical investigation of Fano-like GMR on the size of hole is considered but it is not shown here since it is in the same tendency with the case of changing the hole depth.

As a proof of concept, we design the normal PhC slab structures that induce in the visible region. Here, we realize the same structures and demonstrate their dynamic tunability of colors

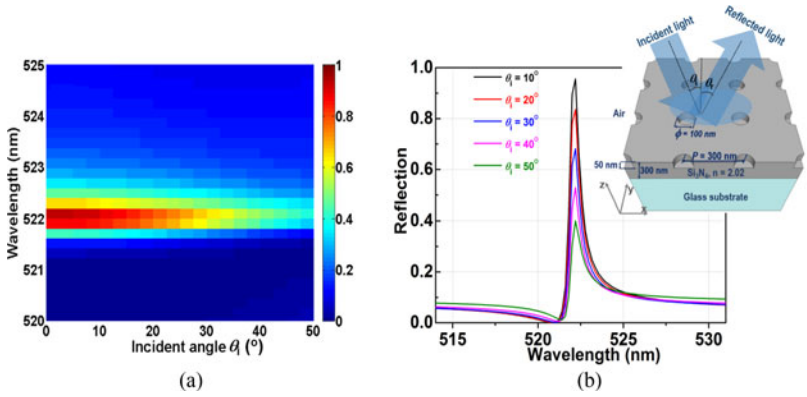

Fig. 2. (a) Simulated angular dependence on the reflection spectra of the structure depicted in inset of (b) for $t = 300$ nm and $\delta = 50$ nm. (b) Example of reflectance peaks caused by Fano resonance for incident angles with $\theta_i = 10°$, $20°$, $30°$, $40°$, and $50°$.

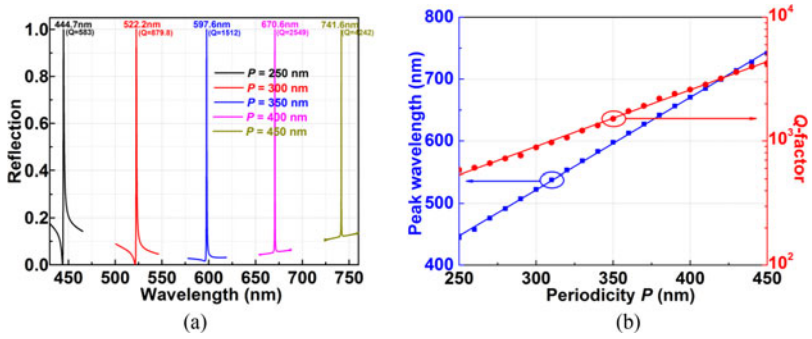

Fig. 3. (a) Simulated reflection spectra of structures with different geometries of the periodicity P for slab thickness $t = 300$ nm and hole depth $\delta = 50$ nm. (b) Evolution of the simulated peak wavelength (blue) and Q-factor (red) as function of periodicity P. As shown in Fig. 3(b), the symbols (squares and spheres) are simulated values and the lines (blue and red) serve as guides.

by varying the periodicity P. Fig. 3(a) shows the simulated reflection spectra of structures with different geometries of the periodicity P for slab thickness $t = 300$ nm and depth $\delta = 50$ nm. As can be seen, when the periodicity P increases, redshift, higher Q-factor, and higher sidebands are achieved. For instance, with the periodicity P of 250 nm and 450 nm, the resonant wavelength λ_R and the corresponding Q-factor are 444.7 nm, 583 and 741.6 nm, 4242, respectively. It means that, as the periodicity P increases, the waveguide mode get less leaky and, hence, the linewidth becomes narrower, leading to an increase of Q-factor. The redshift is caused by the increasing of the effective index of the slab. The mode profile is not shown here; however, the electric field profile indicates that the reflection peak arises from a first order coupling to the TE_0-like mode. The peak wavelength and Q-factor for each resonant mode is evaluated using Fano lineshape and plotted in Fig. 3(b), which show that Q-factor increases and redshifts and linear dependences as periodicity P increases.

3. Proposed PhC Slabs With Additional Air Holes

As mentioned above, sharp Fano-like lineshape or Q-factor of GMRs can be obtained in normal PhC slabs with thick slab waveguide, small size or thin depth holes. Making thin depth or small size holes may raise difficulties for the fabrication technology [33]. Here we introduce the alternative geometry structure to get the higher Q-factor. Fig. 4(a) shows the diagram of the presented PhC slab structure of lattice constant P of 300 nm. The additional holes with depth δ are the same as the basis holes and size ϕ_1 are positioned in the middle of each unit cell of the normal PhC slab of

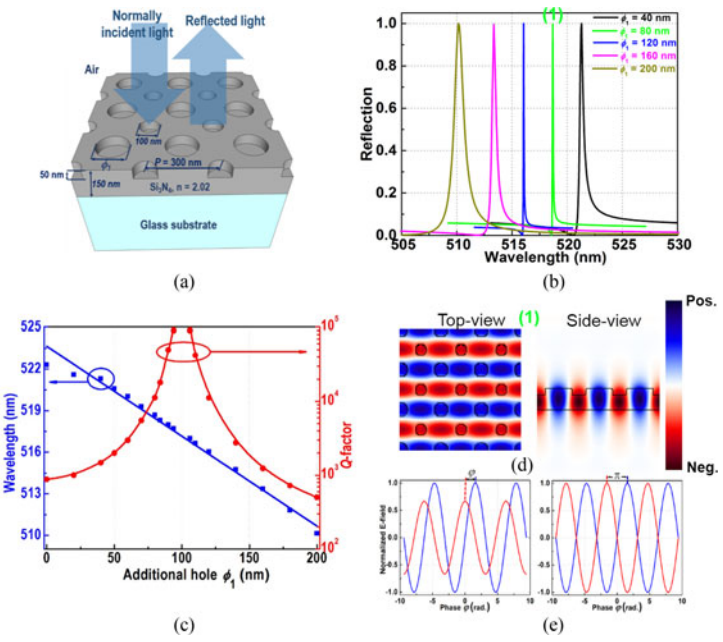

Fig. 4. (a) Sketch of a PhC slab structure generated by using a 2D square lattice of holes as the base and adding an additional hole (ϕ_1) in the centre of each unit cell under normally incident light. (b) Reflection spectra for various additional hole diameters (ϕ_1); (c) evolution of the simulated peak wavelength (blue) and *Q*-factor (red) as function of ϕ_1; (d) shows the electric field distribution along *x* direction at top- and side-views at the resonance for $\phi_1 = 80$ nm; (e) electric field distribution originated from the interaction of the two in-plane waves, which oscillate towards the opposite direction of phase difference of φ.

square lattice. In the calculations in the Fig. 4, the basis hole size ϕ of 100 nm, slab thickness *t* of 150 nm, and depth δ of 50 nm are chosen for simulation. The normal incidence and polarization of TE-like mode is applied.

Fig. 4(b) shows the Fano-like reflection spectra for various size of the additional hole ϕ_1. As ϕ_1 increases, the Fano-like reflection spectrum shifts to the short wavelength due to the decreased effective refractive index of the slab; the linewidth firstly becomes narrower and then becomes broader, that is, *Q*-factor increases firstly and then decreases. Fig. 4(c) shows the evaluation of the simulated peak wavelength (blue) and *Q*-factor (red) as function of additional hole ϕ_1. The symbols (squares and spheres) are simulated values and the lines (blue and red) are the guides for clear views. In the limit where the additional hole ϕ_1 vanishes, i.e., the normal PhC slab, *Q*-factor is 879.8. By adding hole ϕ_1 in the center of each unit cell, the *Q*-factor increases for ϕ_1 increases from 0 to ϕ, for example *Q*-factor $\sim 10^5$ at $\phi_1 = 90$ nm. It is enhanced as a factor larger than two orders of magnitude. If ϕ_1 continues to increase beyond 100 nm, the *Q*-factor decreases. So as ϕ_1 gets closer with ϕ, the Fano GMR gradually diminishes, while the resonance becomes much sharper with decreased linewidth or *Q*-factor enhanced. Particularly, for the case $\phi_1 = \phi = 100$ nm, the guided-mode of alternative PhC slab cannot be directly excited by normal incident light, so the Fano-like resonance disappears. The ϕ_1 also affects the peak wavelength. As shown in Fig. 4(c), the peak wavelength linearly decreases from 522.2 nm for $\phi_1 = 0$ nm to 510.2 nm for $\phi_1 = 200$ nm.

Fig. 4(d) shows the simulated field profiles of top- and side-views of electric field along *x* direction for the resonance indicated in Fig. 4(b). The side-view electric field profile is similar to that shown in Fig. 1(c), which is corresponding to the first order TE_0-like mode. Through the top-view profile, we observe that the electric field distribution is originated from the interaction of the two in-plane waves, which oscillate towards the opposite direction of phase difference of φ [see Fig. 4(e)-left]. At a certain condition, the radiated fields decays each other in the far field. In addition, the coupling between the waveguiding slab and the incident light is reduced due to the interference between the backward and forward waves [34]. This results in the Fano-like resonance with high *Q*-factor. When

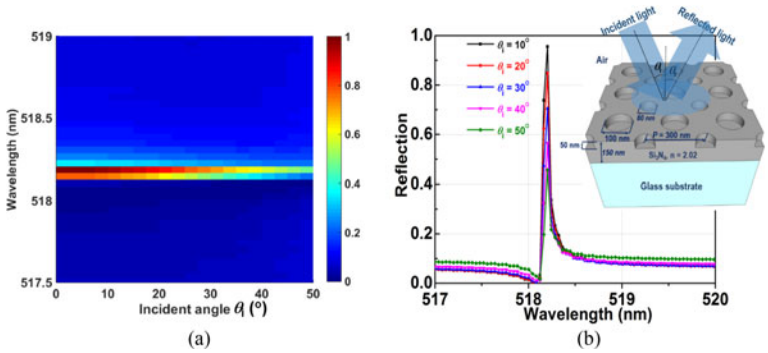

Fig. 5. (a) Simulated oblique angle dependence on the reflection spectra of the structure depicted in inset of (b) for $t = 300$ nm, $\delta = 50$ nm, and $\phi_1 = 80$ nm. (b) Example of reflectance peaks caused by Fano resonance for incident angles with $\theta_i = 10^\circ$, 20°, 30°, 40°, and 50°.

ϕ_1 closes to ϕ, two in-plane waves are oscillated with a phase difference of π and same strength of resonant amplitude [see Fig. 4(e)-right], the two radiated fields strongly cancel each other out in the far field, and the coupling between the waveguiding slab and incident light is largely minimized, very high *Q*-factor can be achieved.

To understand the angular dependence on the optical properties and characteristics, we next calculate the reflection of the proposed PhC slab structure versus the incident angle θ_i. The proposed PhC slab depicted in the inset of Fig. 5(b) with $\phi_1 = 80$ nm is chosen for the simulation. Fig. 5(a) shows the dependence of the incident angle θ_i on the reflection spectra. The red hot spot locates at around 518.2 nm in the figure represents a depthless in reflectivity and hence indicates the presence of a strong optical mode for the incident angle smaller than 30°. The width and blueness of the shaded area indicate the width and strength of the optical mode. Fig. 5(b) shows the example of reflectance peaks caused by Fano-like resonance for incident angles with $\theta_i = 10^\circ$, 20°, 30°, 40°, and 50°. As Fig. 5 shown, the change of incidence angle makes only change the amplitude of reflection doesn't change the resonant wavelength at near 518.2 nm. In addition, the sidebands slightly change when the incident angle changes. The numerical investigation of Fano-like GMR on the size of hole is considered but it is not shown here. It is similar to the reflection spectra of the proposed PhC slabs with the variation of the hole depths, slightly blue-shift and broader linewidth (*Q*-factor decreases) of resonant spectrum when the size of hole increases.

Experimentally, it is possible to fabricate all our designed structures using Focused Ion Beam (FIB) etched into the Si_3N_4 layer. In particular, the Si_3N_4 thin films with different thicknesses ($t =$ 150 nm $\sim$ 300 nm) are deposited on a glass substrate using a thermal evaporator or a Plasma Enhanced Chemical Vapour Deposition (PECVD) techniques. The 2D-PhC slab of the square lattice of the circular holes with diameter (ϕ) and periodicity (P) of 100 nm and 300 nm, respectively, is patterned on the Si_3N_4 layer by a FIB system. The etching depth (δ) can be varied from 30 nm to 70 nm by controlling the FIB current and dwell time. Finally, the 2D-PhC slabs are formed on top of the Si_3N_4 thin films.

4. Conclusions

In conclusion, we numerically investigated the Fano-like GMR color filters using 2D-PhC slabs of square lattice of air holes emphasis on the *Q*-factor and low reflection sidebands. A proposed PhC lattice is presented by introducing an additional hole in each unit cell to enhance the light confinement in the waveguiding slab and the coupling between the waveguiding slab and incident light is largely minimized due to interference between reflected back and forth at the GMR, resulting in a high *Q*-factor of Fano-like GMR in the proposed PhC slab. We believe that our simulation results suggest the promise for photonic device applications such as sensitive optical filters, lasers, biosensors, and also switching/bistability.

References

[1] J. A. Castellano, *Handbook of Display Technology*. New York, NY, USA: Academic, 1992, pp. 299–303.
[2] R. W. Sabnis, "Color filter technology for liquid crystal displays," *Displays*, vol. 20, pp. 119–129, 1999.
[3] S. Kinoshita, S. Yoshioka, and J. Miyazaki, "Physics of structural colors," *Rep. Prog. Phys.*, vol. 71, 2008, Art. no. 076401.
[4] T. Kudo *et al.*, "Pigmented photoresists for color filters," *J. Photopolym. Sci. Technol.*, vol. 9, pp. 109–120, 1996.
[5] Y. Shen, V. Rinnerbauer, I. Wang, V. Stelmakh, J. D. Joannopoulos, and M. Soljačić, "Structural colors from Fano resonances," *ACS Photon.*, vol. 2, pp. 27–32, 2015.
[6] M. J. Uddin and R. Magnusson, "Efficient guided-mode-resonant tunable color filters," *IEEE Photon. Technol. Lett.* vol. 25, no. 24, pp. 1552–1554, Sep. 2012.
[7] A. C. Arsenault, D. P. Puzzo, I. Manners, and G. A. Ozin, "Photonic-crystal full-colour displays," *Nature Photon.*, vol. 1, pp. 468–472, 2007.
[8] W. Wan, J. Gao, and X. Yang, "Full-color plasmonic metasurface holograms," *ACS Nano*, vol. 10, pp. 10671–10680, 2016.
[9] F. Cheng, J. Gao, L. Stan, D. Rosenmann, D. Czaplewski, and X. Yang, "Aluminum plasmonic metamaterials for structural color printing," *Opt. Exp.*, vol. 23, pp. 14552–14560, 2015.
[10] H. Kim *et al.*, "Structural colour printing using a magnetically tunable and lithographically fixable photonic crystal," *Nature Photon.*, vol. 3, pp. 534–540, 2009.
[11] H. Butt, Q. Dai, N. N. Lal, T. D. Wilkinson, J. J. Baumberg, and G. A. J. Amaratunga, "Metamaterial filter for the near-visible spectrum," *Appl. Phys. Lett.*, vol. 101, 2012, Art. no. 083106.
[12] M. J. Uddin and R. Magnusson, "Highly efficient color filter array using resonant Si_3N_4 gratings," *Opt. Exp.*, vol. 21, pp. 12495–12506, 2013.
[13] M. J. Uddin, T. Khaleque, and R. Magnusson, "Guided-mode resonant polarization-controlled tunable color filters," *Opt. Exp.*, vol. 22, pp. 12307–12315, 2014.
[14] B. Michaelis *et al.*, "Generating lithographically-defined tunable printed structural color," *Adv. Eng. Mater.*, vol. 15, pp. 948–953, 2013.
[15] S. Fan, W. Suh, and J. D. Joannopoulos, "Temporal coupled-mode theory for the Fano resonance in optical resonators," *J. Opt. Soc. Amer. A*, vol. 20, pp. 569–572, 2003.
[16] A. E. Miroshnichenko, S. Flach, and Y. S. Kivshar, "Fano resonances in nanoscale structures," *Rev. Mod. Phys.*, vol. 82, pp. 2257–2298, 2010.
[17] Y. Shuai *et al.*, "Double-layer Fano resonance photonic crystal filters," *Opt. Exp.*, vol. 21, pp. 24582–24589, 2013.
[18] Y. Shuai *et al.*, "Coupled double-layer Fano resonance photonic crystal filters with lattice-displacement," *Appl. Phys. Lett.*, vol. 103, 2013, Art. no. 241106.
[19] G. D'Aguanno, D. de Ceglia, N. Mattiucci, and M. J. Bloemer, "All-optical switching at the Fano resonances in sub-wavelength gratings with very narrow slits," *Opt. Lett.*, vol. 36, pp. 1984–1986, 2011.
[20] Q. M. Ngo, K. Q. Le, D. L. Vu, and V. H. Pham, "Optical bistability based on Fano resonances in single- and double-layer nonlinear slab waveguide gratings," *J. Opt. Soc. Amer. B*, vol. 31, pp. 1054–1061, 2014.
[21] Q. M. Ngo, K. Q. Le, T. T. Hoang, D. L. Vu, and V. H. Pham, "Numerical investigation of tunable Fano-based optical bistability in coupled nonlinear gratings," *Opt. Commun.*, vol. 338, pp. 528–533, 2015.
[22] Q. M. Ngo, K. Q. Le, and V. D. Lam, "Optical bistability based on guided-mode resonances in photonic crystal slabs," *J. Opt. Soc. Amer. B*, vol. 29, pp. 1291–1295, 2012.
[23] L. J. Martinez, N. Huang, J. Ma, C. Lin, E. Jaquay, and M. L. Povinelli, "Design and optical characterization of high-Q guided-resonance modes in the slot-graphite photonic crystal lattice," *Opt. Exp.*, vol. 21, pp. 30975–30983, 2013.
[24] J. Ma, L. J. Martinez, and M. L. Povinelli, "Optical trapping via guided resonance modes in a Slot-Suzuki-phase photonic crystal lattice," *Opt. Exp.*, vol. 20, pp. 6816–6824, 2012.
[25] W. Zhou *et al.*, "Flexible photonic-crystal Fano filters based on transferred semiconductor nanomembranes," *J. Phys. D, Appl. Phys.*, vol. 42, 2009, Art. no. 234007.
[26] L. Ferrier, P. Rojo-Romeo, E. Drouard, X. Letartre, and P. Viktorovitch, "Slow Bloch mode confinement in 2D photonic crystals for surface operating devices," *Opt. Exp.*, vol. 16, pp. 3136–3145, 2008.
[27] A. Taflove, *Computational Electrodynamics*. Norwood, MA, USA: Artech House, 1995.
[28] A. Farjadpour *et al.*, "Improving accuracy by subpixel smoothing in the finite-difference time domain," *Opt. Lett.*, vol. 31, pp. 2972–2974, 2006.
[29] M. E. Beheiry, V. Liu, S. Fan, and O. Levi, "Sensitivity enhancement in photonic crystal slab biosensors," *Opt. Exp.*, vol. 18, pp. 22702–22714, 2010.
[30] S. Fan and J. D. Joannopoulos, "Analysis of guided resonances in photonic crystal slabs," *Phys. Rev. B*, vol. 65, 2002, Art. no. 235112.
[31] C. Lin, Z. Lu, S. Shi, G. Jin, and D. W. Prather, "Experimentally demonstrated filters based on guided resonance of photonic-crystal films," *Appl. Phys. Lett.*, vol. 87, 2005, Art. no. 091102.
[32] M. Niraula, J. W. Yoon, and R. Magnusson, "Mode-coupling mechanism of resonant transmission filters," *Opt. Exp.*, vol. 22, pp. 25817–25829, 2014.
[33] M. A Kats, R. Blanchard, P. Genevet, and F. Capasso, "Nanometre optical coatings based on strong interference effects in highly absorbing media," *Nature Mater.*, vol. 12, pp. 20–24, 2013.
[34] W. Zhao, H. Jiang, B. Liu, Y. Jiang, C. Tang, and J. Li, "Fano resonance based optical modulator reaching 85% modulation depth," *Appl. Phys. Lett.*, vol. 107, 2015, Art. no. 171109.